OPEN ACCESS

UNIVERSITY OF DUNDEE

University of Dundee

A Multicellular Model of Intestinal Crypt Buckling and Fission

Almet, Axel A.; Hughes, Barry D.; Landman, Kerry A.; Näthke, Inke S.; Osborne, James M.

Published in:
Bulletin of Mathematical Biology

DOI:
10.1007/s11538-017-0377-z

Publication date:
2018

Document Version
Peer reviewed version

Link to publication in Discovery Research Portal

Citation for published version (APA):
Almet, A. A., Hughes, B. D., Landman, K. A., Näthke, I. S., & Osborne, J. M. (2018). A Multicellular Model of Intestinal Crypt Buckling and Fission. Bulletin of Mathematical Biology, 80(2), 335-359. https://doi.org/10.1007/s11538-017-0377-z

General rights
Copyright and moral rights for the publications made accessible in Discovery Research Portal are retained by the authors and/or other copyright owners and it is a condition of accessing publications that users recognise and abide by the legal requirements associated with these rights.

• Users may download and print one copy of any publication from Discovery Research Portal for the purpose of private study or research.
• You may not further distribute the material or use it for any profit-making activity or commercial gain.
• You may freely distribute the URL identifying the publication in the public portal.

Take down policy
If you believe that this document breaches copyright please contact us providing details, and we will remove access to the work immediately and investigate your claim.

Download date: 05. Apr. 2019

Noname manuscript No.
(will be inserted by the editor)

A multicellular model of intestinal crypt buckling and fission

Axel A. Almet · Barry D. Hughes · Kerry A. Landman · Inke S. Näthke · James M. Osborne

Received: date / Accepted: date

Abstract Crypt fission is an *in vivo* tissue deformation process that is involved in both intestinal homeostasis and colorectal tumourigenesis. Despite its importance, the mechanics underlying crypt fission are currently poorly understood. Recent experimental development of organoids, organ-like buds cultured from crypt stem cells *in vitro*, has shown promise in shedding insight on crypt fission. Drawing inspiration from observations of organoid growth and fission *in vivo*, we develop a computational model of a deformable epithelial tissue layer. Results from *in silico* experiments show the stiffness of cells and the proportions of cell subpopulations affect the nature of deformation in the epithelial layer. In particular, we find that increasing the proportion of stiffer cells in the layer increases the likelihood of crypt fission occurring. This is in agreement with and helps explain recent experimental work.

Axel A. Almet
School of Mathematics and Statistics, University of Melbourne, Victoria 3010, Australia
E-mail: axel.almet@maths.ox.ac.uk *Present address: Mathematical Institute, University of Oxford, Andrew Wiles Building, Radcliffe Observatory Quarter,Woodstock Road, Oxford, OX2 6GG, UK*

Barry D. Hughes
School of Mathematics and Statistics, University of Melbourne, Victoria 3010, Australia
E-mail: barryh@unimelb.edu.au

Kerry A. Landman
School of Mathematics and Statistics, University of Melbourne, Victoria 3010, Australia
E-mail: kerryl@unimelb.edu.au

Inke S. Näthke
Cell and Developmental Biology, School of Life Sciences, University of Dundee, Dundee, DD1 5EH, UK
E-mail: i.s.nathke@dundee.ac.uk

James M. Osborne
School of Mathematics and Statistics, University of Melbourne, Victoria 3010, Australia
E-mail: jmosborne@unimelb.edu.au

This is a post-peer-review, pre-copyedit version of an article published in Bulletin of Mathematical Biology. The final authenticated version is available online at: http://dx.doi.org/10.1007/s11538-017-0377-z

Keywords: epithelia; organoid; deformation; cell stiffness; Chaste

1 Introduction: motivation and background

Crypt fission is a process that leads to an increase in the number of crypts of Liehberkühn, test-tube-shaped invaginations lining the small intestine and colon. These glands maintain the intestinal epithelium, a monolayer of epithelial cells that protects the intestine and facilitates digestion and nutrient absorption (Alberts et al., 2002). Crypt fission is characterised by a bifurcation in the base of the crypt that leads to the eventual branching and formation of two new crypts from the original invagination. It is the mechanism through which crypts multiply (Wright and Alison, 1984; Greaves et al., 2006) and regenerate after tissue damage (Cairnie and Millen, 1975; Wright and Alison, 1984). A more pathological form of crypt fission drives the expansion of adenomas (benign crypt tumours), before further mutations lead to carcinoma development (Preston et al., 2003). This form of crypt fission is characterised by an increased frequency of fission events and asymmetric budding of epithelial tissue from the original crypt that is not witnessed during healthier forms of crypt fission.

Crypt fission normally occurs at the bottom of the crypt, initiating from the round base (Preston et al., 2003). Situated at the base of each crypt are continually-cycling stem cells (Barker et al., 2007) that divide to produce daughter cells. These daughter cells migrate upwards and out of the crypt in a 'conveyor belt' fashion, dividing several more times before differentiating into non-dividing cells with specialised functions to help absorb nutrients or facilitate the transport of matter through the intestines. These terminally differentiated cells sit along the top of the crypts until they eventually undergo apoptosis or are shed into the lumen, the inner intestinal cavity. In the small intestines, differentiated Paneth cells unusually remain at the base, positioned between stem cells. These cells, which are larger, stiffer and more adherent to the basement membrane than stem cells (Langlands et al., 2016), are known to provide essential signals in maintaining the intestinal stem cell niche (Sato et al., 2011). While Paneth cells are not present in the colon, there are 'Paneth-like' cells in the colonic crypt base (such as cKit$^+$ cells) that are suspected to have a similar function (Sato et al., 2011; Rothenberg et al., 2012).

Paneth cells are also hypothesised to have a role in the onset of crypt fission (Sato et al., 2009; Snippert et al., 2013). Recent work by Langlands et al. (2016) showed that the spatial distribution of stem and Paneth cells in the crypt base, their biomechanical differences, and Paneth cell numbers were important factors in the initiation of fission. This experimental work was supported by computational modelling of an epithelial layer, which we will discuss in more detail shortly.

Lining each crypt is the basement membrane, a thin layer of extracellular matrix proteins that form an intricate network of fibres. The basement membrane is important for providing mechanical support and stability to the crypt

(Wright and Alison, 1984; Alberts et al., 2002). There is also evidence to suggest that adhesion between the crypt epithelium and the basement membrane plays a role in cell migration and polarity (Trier et al., 1990). Underneath the basement membrane is connective tissue stroma, consisting of mesenchymal cells, further providing structural support and separating neighbouring crypts.

Despite its obvious clinical significance, there has been a struggle to identify the biomechanical factors responsible for the onset of crypt fission. Part of the elusive nature of crypt fission stems from the historical lack of tractable experimental systems in which crypt fission can be observed, as crypt fission in adult mammals is rare (Wright and Alison, 1984; Park et al., 1995). However, Sato et al. (2009) developed a method for culturing crypt-like structures, called organoids, *in vitro* using isolated stem cells. These cell cultures expand from single cells in a radially symmetric manner, initially resembling spheroids, with a lumen full of apoptotic cells surrounded by a proliferative epithelium. Eventually, instabilities develop along the epithelium, resulting in the formation of outward-protruding buds that resembled crypts. The authors noted that stem and Paneth cells were always found at the sites of budding and that these buds formed in a manner reminiscent of crypt fission (Sato et al., 2009). Hence, if one were able to understand how crypt fission occurred in these *in vitro* organoids, one may be able to shed light on the *in vivo* fission process. We used these observations made by Sato et al., when developing the crypt deformation framework presented in this paper.

Mathematical and computational modelling have been used to study crypt buckling and fission and provide biologically plausible hypotheses. One of the first models of crypt buckling was by Drasdo and Loeffler (2001), who employ a discrete, individual-based model, modelling the crypt as a U-shaped chain of cells. By contrast, Edwards and Chapman (2007) use a continuum approach, modelling the crypt monolayer as a beam. The Edwards and Chapman model was extended by Nelson et al. (2011) to examine the buckling of an epithelial layer on a thin, flexible substrate in parallel with *in vitro* experiments. Similarly, Hannezo et al. (2011) model the intestinal epithelium and the underlying tissue stroma as continuous elastic media to investigate villi formation. Although there are predominantly continuum models of crypt buckling in the literature, there are some computational models. For example, Buske et al. (2012) extend a previous model of the crypt — Buske et al. (2011) — to investigate organoid deformation. Most recently, Pin et al. (2015) model individual cell deformability using fluid mechanics models and vary the material properties of stem and Paneth cells to initiate fission in the crypt base.

While these models have provided insight into the possible biomechanical contributions to crypt fission, a number of these models impose biologically unrealistic constraints by assuming a fixed geometry. One model seeking to overcome this is that of Dunn et al. (2012a). In Dunn et al. (2012a), a two-dimensional off-lattice cell-centre model of a crypt cross section is presented. By modelling the presence of the basement membrane through a curvature-

dependent force, the authors can deform an initially flat epithelial monolayer into a test-tube-shaped crypt, reminiscent of crypt fission during embryogenesis (Cheng and Bjerknes, 1985). Using this deformable crypt model, the authors suggest a mechanism for cell migration in the crypt and show that the frequency of cell death through anoikis is higher in more curved parts of the crypt.

The Dunn et al., model was recently built upon and extended to represent a deformable epithelial layer comprising stem and Paneth cells to study crypt fission (Langlands et al., 2016). In this paper, we present a more complete investigation of the new epithelial layer model and its biomechanics regarding crypt fission. Furthermore, we present a more abstracted framework than the one used in Langlands et al. This retains a certain level of generality within the model and allows us to interpret our findings in the context of either *in vivo* crypts (in the small intestine or colon) or *in vitro* organoids.

The remainder of this paper is structured as follows. In Section 2, we present the components of our model, and the methods used. We then present the results obtained from *in silico* experiments and subsequent analysis in Section 3. These results are discussed in Section 4, along with biological implications and possible directions for future work.

2 Methods

Here, we extend the crypt model outlined in Dunn et al. (2012a) to represent the cross section of a confluent epithelial layer, as originally presented in Langlands et al. (2016). As in Dunn et al., we implement a two-dimensional off-lattice cell-centre model, defining cell shapes by a Voronoï tessellation and cell connectivity through a Delaunay triangulation (Aurenhammer et al., 2013). The edges of the triangulation define the springs along which interactive forces between cells are applied.

In the following sections we present the individual components of the model: the geometry; the applied forces; and the model for cell proliferation and death.

2.1 Geometry

We adopt the same geometry as in Langlands et al. (2016) and consider an approximately circular epithelial layer surrounded by non-epithelial cells. Each cell is initially a hexagon of unit side length (a common starting configuration for Voronoï tessellation models). Investigations are conducted in a rectangular array of cells, where the numbers of cells in the vertical and horizontal directions are chosen such that the height and width of the region are both 20 cell diameters. In this model, space is non-dimensionalised by typical cell diameter, $10\mu m$. The slab initially consists of a connected layer of proliferative epithelial cells surrounded by terminally differentiated non-epithelial cells.

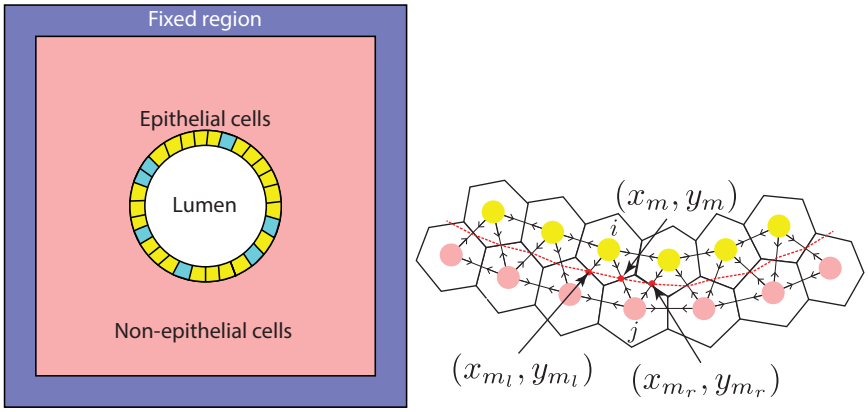

(a) Model Domain (b) Forces between cells

Fig. 1 Model schematics. (a) The geometry of the epithelial layer model. The key features of the computational model have been labelled. Epithelial cells are separated into two populations, with different mechanical properties, shown in light blue and yellow. (b) How the forces are defined in the epithelial layer model. The arrows along the edges of the Delaunay triangulation represent the linear spring forces exerted by each cell in the model. The red dashed line shows how the basement membrane is defined as a confluent piecewise-linear curve along the midpoints of springs springs connecting epithelial (yellow) and non-epithelial (pink) cells. The points used to calculate the discrete curvature κ_{ij} at the midpoint (x_m, y_m) between epithelial centre i and non-epithelial centre j have been marked.

These non-epithelial cells could represent either the Matrigel surrounding an organoid or the surrounding tissue stroma of a crypt (as in Dunn et al. (2012a) and Langlands et al. (2016)). Figure 1(a) shows the initial configuration of the model, which may represent the initial cystic geometry of organoids or the conjoining of two crypt bases. To simulate the lumen, the region enclosed by the epithelial layer is filled with with 'ghost nodes'. These nodes do not exert a force on 'real nodes' such as the epithelial and non-epithelial cells—hence their name—but can conversely experience forces due to real node neighbours. However, by placing ghost nodes inside the void, the formation of excessively long connections between cells in the ring, which would occur when calculating the Delaunay triangulation, is prevented (see Van Leeuwen et al. (2009)). This in turn prevents large spring forces occurring. For this reason, layers of ghost nodes are also placed around the outside, allowing outer edges of the mesh, as defined by real nodes, to maintain a convex hull.

Additional layers of non-epithelial cells are fixed around the edges of the square region to ensure the total area of the box remains constant during simulations. This ensures that the epithelial layer is able to deform without compromising the overall shape of the box. This has the same effect as having a periodic domain representing multiple adjacent crypts or organoids.

2.2 Forces

Cells in the model are subjected to the same forces used in Dunn et al. (2012a,b) and Langlands et al. (2016). A linear, over-damped spring force law is used to model attraction and repulsion between cells, where the springs are defined by the edges of the Delaunay triangulation. Moreover, the basement membrane force formulated by Dunn et al. (2012a,b) is applied along the midpoints of springs connecting epithelial and non-epithelial cells. This has been summarised in Figure 1(b). This is analogous to previous applications of the force between epithelial and stromal cells (Dunn et al., 2012a,b).

The equation of motion of each cell can be described using Newton's second law. As cells move in dissipative environments of extremely small Reynolds numbers (Dallon and Othmer, 2004), we can consider the inertial terms as negligible in comparison to the drag and cell-cell interaction terms. Using $\mathbf{r}_i(t)$ to denote the position of cell centre i at time t, the resulting force balance is

$$\eta_i \frac{d\mathbf{r}_i}{dt} = \sum_{j \in N_i(t)} \mu_{ij} \left(\|\mathbf{r}_{ij}(t)\| - l_{ij}(t) \right) \widehat{\mathbf{r}}_{ij}(t) + \mathbf{F}_i^{BM}. \tag{1}$$

This system of first-order ordinary differential equations is solved using a Forward Euler time-stepping method. Appropriate measures are placed to prevent instabilities arising from the explicit numerical integration method. Moreover, the time step Δt is chosen so that reducing the size of Δt does not change simulation results.

The term on the left-hand side of Equation (1) represents the viscous force, assumed to be proportional to the velocity of node i and independent of other forces. Here, η_i is the drag coefficient, which can depend on cell type.

The first term on the right-hand side of Equation (1) describes the elastic interaction force between cells, modelled by Hooke's law and assumed to act in the opposite direction to the drag force. The constant μ_{ij} is the stiffness of the spring connecting nodes i and j; $\mathbf{r}_{ij}(t) = \mathbf{r}_j(t) - \mathbf{r}_i(t)$ with corresponding unit vector $\widehat{\mathbf{r}}_{ij}(t)$; and $l_{ij}(t)$ is the resting spring length, which depends on both cell type and age.

Finally, $\mathbf{F}_i^{BM}$ denotes the basement membrane force and is based on a local curvature calculation and was first presented in Dunn et al. (2012b). In summary an additional force is imposed in order to drive the monolayer to attain a certain curvature. It is applied only to epihelial cells; that is, if cell i is a non-epithelial cell, then $\mathbf{F}_i^{BM} = 0$.

Following Dunn et al. (2012b), $\mathbf{F}_i^{BM}$ is defined to be

$$\mathbf{F}_i^{BM} = \beta \sum_j \left(\kappa_{ij} - \frac{1}{R} \right) \widehat{\mathbf{u}}_{ij}, \tag{2}$$

where β is the basement membrane force parameter, characterising the stiffness of the basement membrane and how strongly the epithelial cell adheres to the basement membrane; $\widehat{\mathbf{u}}_{ij}$ is the unit vector from the non-epithelial node j to the epithelial node i; κ_{ij} is the discrete curvature calculated at the

non-epithelial-to-epithelial spring midpoint and $1/R$ is the target curvature, representing the spontaneous curvature of a circle of radius R. Note that a curvature of $1/R = 0$ corresponds to a flat monolayer as considered in Dunn et al. (2012b), formally it can be considered as the limit $R \to \infty$, where $1/R \to 0$.

The discrete curvature κ_{ij} is defined by a discretisation of the formula (Dunn et al., 2012b)

$$\kappa(s) = \frac{x'_{BM}(s)y''_{BM}(s) - x''_{BM}(s)y'_{BM}(s)}{(x'_{BM}(s)^2 + y'_{BM}(s)^2)^{\frac{3}{2}}}\ , \tag{3}$$

where $(x_{BM}(s), y_{BM}(s))$ denotes the line connecting the midpoints of the epithelial-to-non-epithelial springs, parametrised by the arc length s. In order to calculate the curvature, suppose the that the current midpoint between the i^{th} epithelial node and j^{th} non-epithelial node is given by $(x_m, y_m) = ((x_i + x_j)/2, (y_i + y_j)/2)$. We approximate the first and second derivatives using central differences (Süli and Mayers, 2003) applied on the midpoint to the left, (x_{m_l}, y_{m_l}), and the right, (x_{m_r}, y_{m_r}) (see Figure 1(b)), as follows:

$$x'_m \approx \frac{x_{m_r} - x_{m_l}}{\Delta s_l + \Delta s_r}, \tag{4}$$

$$x''_m \approx 2\left[\frac{\Delta s_l x_{m_r} - (\Delta s_l + \Delta s_r)x_m + \Delta s_r x_{m_l}}{\Delta s_l \Delta s_r(\Delta s_l + \Delta s_r)}\right], \tag{5}$$

with analogous formulae for y'_m and y''_m. Where Δs_l and Δs_r are the distances between the midpoints

$$\Delta s_l = \sqrt{(x_m - x_{m_l})^2 + (y_m - y_{m_l})^2}. \tag{6}$$

$$\Delta s_r = \sqrt{(x_{m_r} - x_m)^2 + (y_{m_r} - y_m)^2}. \tag{7}$$

The application of a basement membrane force in an organoid model is supported by the observation that Matrigel is comprised mostly of the protein laminin, the same protein that largely makes up the basement membrane. Furthermore, Matrigel is a viscoelastic mixture (Zaman et al., 2006): as cells are subjected to viscoelastic interaction forces, this justifies our use of non-dividing cells to represent both Matrigel and stromal cells in our model.

2.3 Cell birth and death

In order to model continuous growth of the epithelial layer, epithelial cells are able to proliferate *ad infinitum*. Each proliferative cell divides according to a stochastic cell cycle duration that follows a uniform $U(12, 14)$ distribution in hours (Alberts et al., 2002). For each simulation, we re-seed the pseudo-random number generator before varying model parameters of interest. This means that for each parameter combination, we have a sequence of independent birth events. Moreover, the same seeds are used for each parameter combination, allowing us to run identical experiments and compare model behaviour accurately.

Upon division, a cell is replaced instantaneously by two daughter cells connected by a spring lying in a randomly chosen direction (with other springs assigned by the Delaunay triangulation). Initially the daughter cells are placed a small distance of 0.05 cell diameters away from the original parent cell in opposite directions. The newly-created spring is assigned a resting spring length of $l_{ij}(t)$ that increases linearly from 0.1 to 1 over one hour. This models the growth of cells during division events and prevents unrealistic large forces arising from proliferation. Note that this is different to the planar cell division mechanism employed in the works of Dunn et al. (2012a,b), but is the same as that employed in Meineke et al. (2001) and Van Leeuwen et al. (2009).

To prevent over-crowding and to maintain confluency in the layer, cell death in the form of anoikis is introduced. If any epithelial cell loses all connection to the surrounding non-dividing cells, as determined by the underlying Delaunay triangulation, and enters the lumen, it is removed from the simulation. This is equivalent to the cell losing contact with the basement membrane in previous implementations of anoikis (Galle et al., 2005; Buske et al., 2011; Dunn et al., 2012a,b).

2.4 Computation

All developments of the model were performed within the Chaste framework (Pitt-Francis et al., 2009; Mirams et al., 2013). Chaste (Cancer, Heart and Soft Tissue Environment) is a software library for multiscale simulations of biological phenomena with an emphasis on modelling multicellular tissue populations. Historically, applications of cell-based models in Chaste have been focused on crypt modelling and colorectal carcinogenesis (Van Leeuwen et al., 2009; Osborne et al., 2010; Dunn et al., 2012a,b, 2013). Chaste is an open-source simulation package and can be accessed from `http://www.cs.ox.ac.uk/chaste/`. The code for this project can be found at `https://chaste.cs.ox.ac.uk/trac/wiki/PaperTutorials/EpithelialFission`.

In each stage of model development, simulations were run long enough to guarantee steady state convergence in the absence of mechanical instability. A typical simulation of the most complex variant of the model, run for 100 hours (scaled by cell cycle time) requires approximately 13 minutes of CPU time on a single core of a desktop Linux PC with an Intel Xeon E5-4650 processor.

2.5 Determining fission occurrence

In order to determine occurrences of crypt fission, a measure of shape complexity is required. We measure the *circularity* (Žunić and Hirota, 2008) of the layer, a dimensionless quantity defined by

$$C(t) = \frac{4\pi A(t)}{P(t)^2}, \ 0 \leq t \leq T, \tag{8}$$

where $A(t)$ and $P(t)$ are the area and perimeter of the cross section of the epithelial layer respectively at time t. Both the area $A(t)$ and the perimeter $P(t)$ can be calculated using explicit formulae. For an epithelial ring comprising $N(t)$ cells, where the positions of the cell centres are given by (x_i, y_i), $i = 1, \ldots, N(t)$, in clockwise or anti-clockwise order,

$$A(t) = \frac{1}{2}\left|\sum_{i=0}^{N(t)} (x_i y_{i+1} - x_{i+1} y_i)\right|, \tag{9}$$

$$P(t) = \sum_{i=0}^{N(t)} \sqrt{(x_{i+1} - x_i)^2 + (y_{i+1} - y_i)^2}. \tag{10}$$

To close the ring, we impose the condition $(x_{N(t)+1}, y_{N(t)+1}) = (x_1, y_1)$. The derivation of the formula for $A(t)$ follows from a straightforward application of Green's theorem.

It is clear from Equation (8) that a circle has a circularity value of one. Moreover, since a circle has the minimum perimeter amongst all shapes with the same area, we can see that $0 < C(t) \leq 1$. Figure 2 depicts different epithelial layer shapes from simulations and the corresponding circularity values. We can see that shapes with more circular forms will have circularity values closer to one, while more complex shapes will have circularity values closer to zero. Moreover, initial computational experiments also showed that once an organoid had deformed sufficiently to say that crypt fission had occurred, it would not deform back to a circular shape. From these observations, we formulate our criterion for fission events as follows: in a simulation running for T hours, we say that crypt fission has occurred if $C(T) < 0.5$.

2.6 Preliminary simulations and parameter selection

In silico experiments were run to determine the effects of the basement membrane force parameters β and $1/R$ on the shape of the epithelial layer. The parameter β quantifies adhesion to the basement membrane while $1/R$ describes the ideal local curvature of the layer. All other model parameter values are displayed in Table 1. Each simulation started with an initial lumen radius of 2.5 cell diameters to provide the epithelial tissue with enough space to grow and change without being overly affected by the imposed boundaries. While there will be some influence on the shape of the layer due to the boundaries of the domain, for some parameter choices. The qualitative results presented here are unchanged in a larger domain. The aim of these initial experiments was to deduce a pair of β and $1/R$ values that yield a circular steady state in the case of mechanical homogeneity, which could be perturbed in further experiments.

Figure 3 displays the final state (at $T = 60$ hours) of the epithelial layer for typical simulations using different combinations of β and $1/R$. Examining the layers along the bottom row, when $1/R = 0$, we see that increasing β

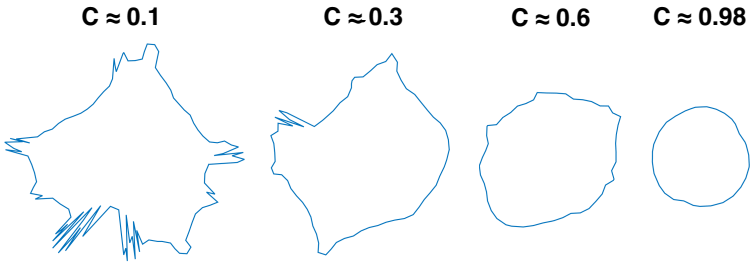

Fig. 2 Examples of different circularity values. The shapes have been taken from different simulations. We see that for more deformed shapes, the circularity value is closer to zero.

eventually snaps the layer. This behaviour is expected: if $1/R = 0$, then the epithelial layer is attempting to be locally flat everywhere, which can only occur by breaking the layer's confluency. This suggests that for higher values of β, a non-zero target curvature is required for a stable shape as can be seen by the first and second row of the figure and this is shown in the middle row for $1/R = 0.2$. However, if $1/R$ is too high, the layer grows excessively and the epithelial cells are pushed to the boundaries of the domain, as seen in the top row of Figure 3. This prevents us from being able to observe the effects of any mechanical perturbations to the system. Intuitively, as we increase the local target curvature, one would expect the resulting epithelial layer to be smaller, this is not the case here as, for a larger local target curvature, the layer is locally trying to have a higher curvature resulting in a larger outward force and resulting in a larger layer, moreover, this behaviour is exaggerated by increasing β as the outward force is even larger.

Therefore, out of the values we investigated, we set the target curvature to be $1/R = 0.2$. Furthermore, to ensure that the epithelial layer will converge to a stable circle, while not being overcrowded with epithelial cells, we set the basement membrane stiffness to be $\beta = 10$. We fix $\beta = 10,\ 1/R = 0.2$ for all further investigations. We note that the use of a different-sized domain would not make a qualitative difference in results. For example, for a larger domain, we could simply increase $1/R$ further until we observed the same behaviour.

Parameter	Values	Units	Reference
μ (spring stiffness)	15	N Cell diameter^{-1}	Meineke et al. (2001)
η (constant drag coefficient)	1	N hours Cell diameter^{-1}	Meineke et al. (2001)
l_{ij} (equilibrium spring rest length)	1	Cell diameter	Van Leeuwen et al. (2009)
Δt (timestep)	0.005	Hours	
β (basement membrane stiffness)	5–15 (10)	N Cell diameter^{-1}	
κ_{ij} (local discrete curvature)	See text	Cell diameter^{-1}	
$1/R$ (target curvature)	0–0.8 (0.2)	Cell diameter^{-1}	

Table 1 Model parameters and values. Distances are measured by the natural cell diameter $10\mu m$ (Alberts et al., 2002), time has been scaled by hours and mechanical variables have been scaled so that $\eta = 1$. For parameters with a range of values, the default values used in investigations are stated in brackets. Any parameter not mentioned in this table will be non-dimensional.

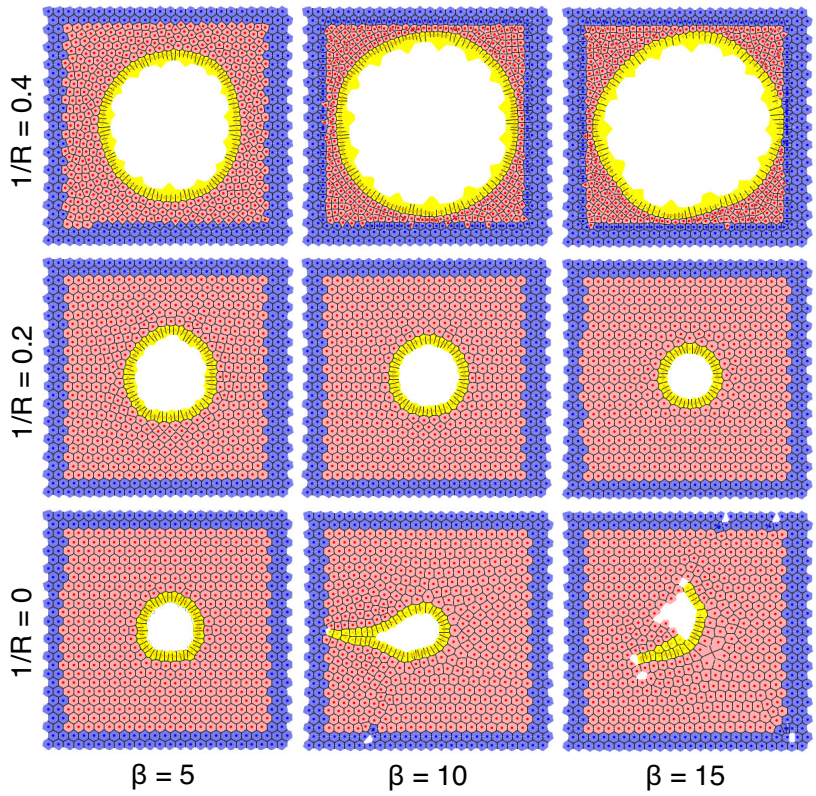

Fig. 3 The effect of the basement membrane on epithelial layer shape. The state of the epithelial layer after 60 simulation hours (already in steady state if it exists) has been shown for various values of the basement membrane stiffness β and the target curvature $1/R$. The white gaps amongst the non-epithelial region in some of the images are ghost nodes that have been forcibly moved out of the lumen due to force instabilities. The protrusions from the epithelial layer into the lumen along the top row are a consequence of the tessellation, as the distance between ghost nodes and epithelial cells is increase for higher values of $1/R$.

Based on these preliminary simulations, all subsequent results presented in the paper were averaged over 100 simulations, where each simulation was run for, and the circularity calculated at, 100 hours. This time length was chosen as it allowed for the convergence to a steady state shape, if it existed. This time length is also in accordance with the time it takes organoids to bud (Sato et al., 2009). Results are unchanged if we run for a longer time.

2.7 Introducing heterogeneous cells

Motivated by the presence of both stem and differentiated secretory cells in crypt bases and organoid buds, and by the observation that these cells are stiffer, more adhesive and larger than stem cells, we introduce mechanically

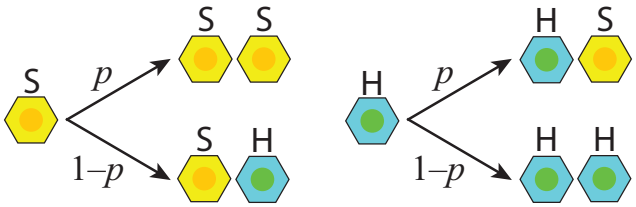

Fig. 4 The new division rule for epithelial cells. Both hard and soft cells can divide, producing one cell identical to the parent cell and another cell that is a soft or hard cell with probabilities p and $1-p$ respectively. This division rule results in an expected soft cell proportion of p.

different cells into the cell population. While previous models have incorporated multiple cell types (Buske et al., 2011; Pin et al., 2012, 2015), many models fail to account for the physical differences between these cell types. In this model, we will focus on modelling the relative stiffness of two different cell types that we will call 'hard' and 'soft'. This is defined through the spring stiffness constant μ_{ij} connecting cell i and cell j, which appears in the intercell force law in the right–hand side of Equation (1). If both cell i and j are soft cells, then we define $\mu_{ij} := \mu_S = \mu$. However, if at least one of cells i or j is a hard cell, we define $\mu_{ij} := \mu_H$. By construction, we must have $\mu_H > \mu_S$. The *stiffness ratio* μ_H/μ_S, quantifying relative stiffness, is thus defined as a new simulation parameter. In Pin et al. (2015), the authors used Atomic Force Microscopy measurements to show that the Young's modulus of Paneth cells is approximately four times greater than stem cells, suggesting that $\mu_H/\mu_S = 4$, where Paneth and stem cells are hard and soft cells respectively. In order to capture the transition from homeostasis to buckling accurately, we performed investigations for $3 \leq \mu_H/\mu_S \leq 5$. We note that apart from the different spring stiffnesses, hard cells are otherwise identical to soft cells in our simulations. This allows us to interpret model results in a variety of biological contexts relevant to both crypt homeostasis and colorectal cancer.

2.8 Controlling cell numbers

In our model, during mitosis, an epithelial cell will produce one daughter cell identical to the parent, and an additional soft cell with probability p or an additional hard cell with probability $1-p$. This division rule is summarised in Figure 4. In mechanically homogeneous populations obeying this rule, the expected proportion of soft cells will be p. However, in this system, the influence of other parameters such as the stiffness ratio μ_H/μ_S will affect the actual proportion of soft cells. Hence, we call the parameter p the *target proportion*. All model investigations were performed for $0.25 \leq p \leq 0.95$.

Initially, hard cells were modelled as non-dividing, differentiated cells in the epithelial layer, mimicking non-stem crypt base cells (Wright and Alison, 1984; Alberts et al., 2002). Preliminary experiments showed that for $\mu_H/\mu_S \geq 4$,

budding could be initiated. Furthermore, the buds typically formed when a soft cell was pushed out into the non-epithelial region by neighbouring hard cells, a mechanism not unlike that seen in Pin et al. (2015). However, the cross-sectional geometry of the model does not allow for cell sorting. This caused hard cells to push the majority of neighbouring soft cells into the lumen, subjecting them to anoikis. Eventually the epithelial layers became monoclonal with hard cells, preventing any exploring of cell patterning in the model. This led to the introduction of the cell division rule.

Parameter sweeps over the target proportion p and the stiffness ratio μ_H/μ_S were performed to investigate the effect of mechanical heterogeneity on actual soft cell proportions. For each $(\mu_H/\mu_S, p)$ pair, 200 simulations were run for 100 hours each, allowing enough time for either crypt fission or steady state convergence to occur. Recalling that our criterion for fission occurrence is dependent on the final circularity $C(100)$, if $C(100) \geq 0.5$ then the epithelial layer is assumed to be in steady state. This assumption is based on the observation that an epithelial layer undergoing fission can never be in a steady state, as buds have the potential to grow *ad infinitum* in the model.

For each value of μ_H/μ_S, we model the relationship between the target proportion p and the final soft cell proportion, calculated as an average of simulation results. In order to take an accurate average of data, final proportion averages are only accepted if they were drawn from samples with a size of at least 50. Hence, for a $(\mu_H/\mu_S, p)$ pair, the average final stem cell proportion is only accepted if the model has converged to a steady state at least 50 times (out of 200 runs).

Mechanical heterogeneities in the epithelium and cell death mean that the final soft cell proportion does not follow a linear relationship with the target proportion p. Figure 5 shows the non-linear relationship between the target proportion and the final soft cell proportion for several values of μ_H/μ_S. Based on form, the final proportion is modelled as a cubic function of the target proportion, calculated using least squares regression (Björck, 1996). However, the relationship between the final and target soft cell proportion does not significantly change for different values of μ_H/μ_S, as seen in Figure 6. The μ_H/μ_S-dependence can then be removed by fitting a cubic to the full set of accepted final soft cell proportion values (also shown in Figure 6). With this cubic function, for a given final soft cell proportion value, the target proportion parameter p required to produce the corresponding *in silico* proportion can readily be obtained and therefore simulations with any desired composition can be run and investigated.

3 Results

In this section, we present the findings from *in silico* experiments, using the model and methods described in Section 2. Our results focus primarily on the effect of varying the biomechanical properties—mainly the relative cell

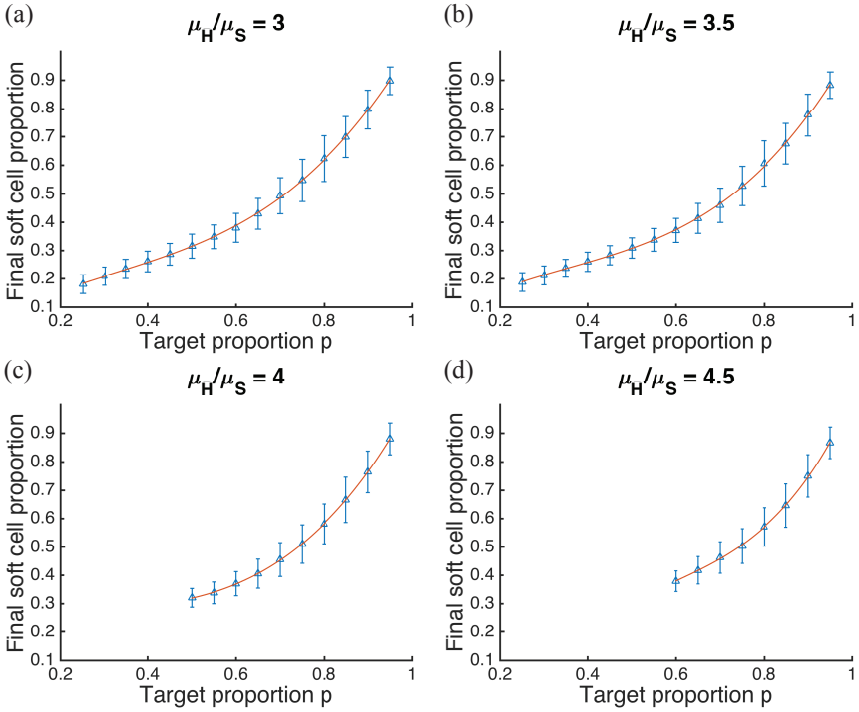

Fig. 5 The relationship between final and target stem cell proportion. Plots of the average final stem cell proportion (blue triangles) versus the target proportion p for stiffness ratio μ_H/μ_S values of (a) 3, (b) 3.5, (c) 4 and (d) 4.5. The bars show the standard deviation from the mean proportions. For each value of μ_H/μ_S, a cubic (red line) has been fitted to each set of data. Note that as μ_H/μ_S increases, we have a smaller set of data points to which we can fit the data, due to the increased likelihood of crypt fission for low proportions of stem cells.

stiffness—of epithelial cells on the nature of crypt buckling and fission and how tissue deformation in turn affects cells within the epithelial layer.

3.1 Likelihood of crypt fission

We observe that crypt fission is more likely to occur for higher stiffness ratio values; that is, when hard cells are much stiffer than soft cells. Although this may be expected, when examining the simulation results in their entirety, the contours of fission probabilities reveals a more complex relationship between the proportion of soft cells and the relative stiffness of hard cells than one would have anticipated. Figure 7 shows the probability of fission for different soft cell proportions and stiffness ratio values. We see in Figure 7 that an approximately elliptic border divides the region where crypt fission never occurs from the region where the epithelial layer always buckles. Furthermore, we observe that different combinations of soft cell proportions and stiffness ratios can lead to

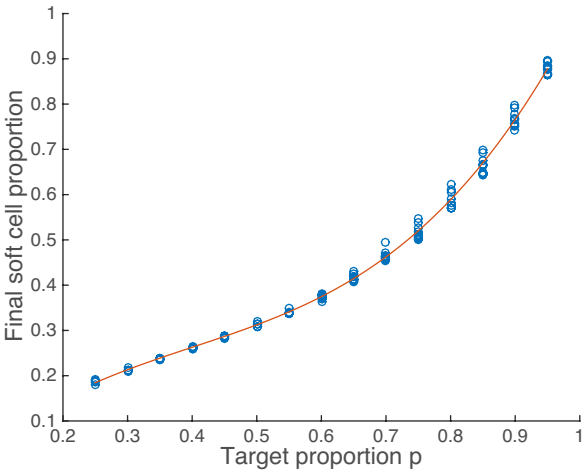

Fig. 6 The set of accepted steady state soft cell proportions and the fitted cubic. The red line represents the fitted cubic and the blue circles represent the soft cell proportions calculated from simulation data. We can see that the actual final proportion does not appear to change greatly for different μ_H/μ_S values. Furthermore, both the data and the fits are well within the standard deviation bounds shown in Figure 5.

the same physical behaviour. For example, an epithelial layer with a very low proportion of soft cells and hard cells of moderate stiffness may show the same behaviour as a layer with a higher proportion of soft cells but much stiffer hard cells.

An interesting phenomenon is observed when analysing the probabilities of fission. For low values of μ_H/μ_S, the probability is zero everywhere, as expected. However, for higher values of μ_H/μ_S, the fission probability appears to follow a sigmoidal relationship with the target proportion p. As μ_H/μ_S increases, a travelling wave of probability functions in the μ_H/μ_S parameter space emerges. This is demonstrated in Figure 8, where the probabilities of fission are plotted for several values of μ_H/μ_S. To exploit this apparent correspondence between the probability of fission and p, we model the relative frequency data using a logistic curve (Hosmer Jr and Lemeshow, 2004) for each value of μ_H/μ_S, fitted through least squares. Note that a logistic regression was used solely on the basis of form and not because of any underlying statistical assumption about the data. Analysis of the modelled logistic curves reveals that the inflection points of each logistic curve follows a non-linear relationship with the stiffness ratios μ_H/μ_S, shown in Figure 9(a). The set of inflection points is fitted to a function of the form $f(\mu_H/\mu_S) = a(\mu_H/\mu_S)^b + c$, also plotted in Figure 9(a). We fit the model only to points where the probability wave starts to develop sufficiently (for $\mu_H/\mu_S > 3.55$). While the steepness coefficient of each logistic function is not as straightforward to model (Figure 9(b)), we can construct adequate approximations to the original models by taking the average coefficient value with the corresponding inflection point

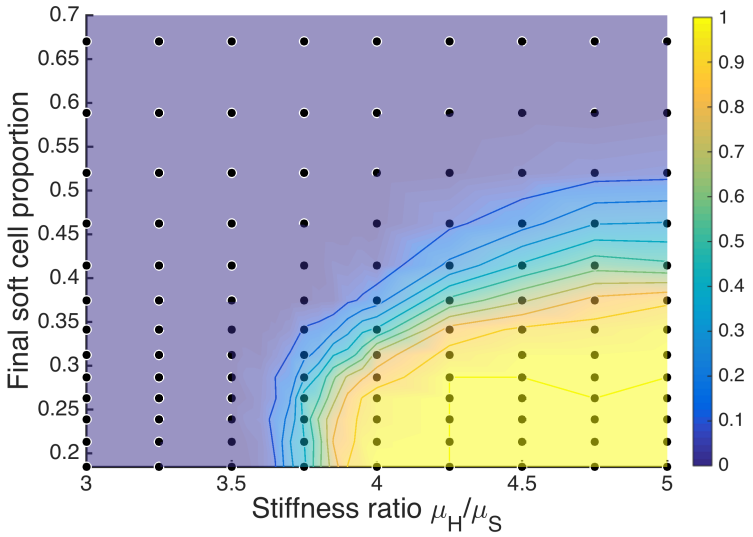

Fig. 7 The empirical probability of crypt fission. A contour of the probabilities of crypt fission for various values of the stiffness ratio μ_H/μ_S and steady state soft cell proportion. Regions of dark blue represent probabilities of zero, while regions of yellow represent probabilities of one. Points obtained from simulation data are marked with black circles. There is a clear divide between areas of zero probability and areas of certain fission.

obtained from the fitted curve. These interpolated fits permit the probability of fission to be represented as a smoothly varying function of the target proportion p and the stiffness ratio μ_H/μ_S. Given the data set, one may also be inclined to take a linear approximation for the steepness coefficient, as shown in Figure 9(b). However, for $\mu_H/\mu_S < 3.5$, the steepness coefficient would become non-negative, resulting in an inaccurate fit for lower stiffness ratio values. Note that even for $\mu_H/\mu_S > 3.5$ the subsequent results presented here for the constant fit are extremely close to those for the linear fit (not included for brevity), hence we choose to use the constant fit.

In conjunction with the cubic function derived previously (Section 2.8), for any pair of final soft cell proportion and stiffness ratio values, the probability of crypt fission can be calculated exactly, avoiding the need for any further computational effort. A full continuum surface of the probabilities can therefore be produced. Figure 10 demonstrates that the surface captures the qualitative behaviour of the original simulation results effectively. In particular, the position and shape of the border dividing homeostasis and buckling is retained.

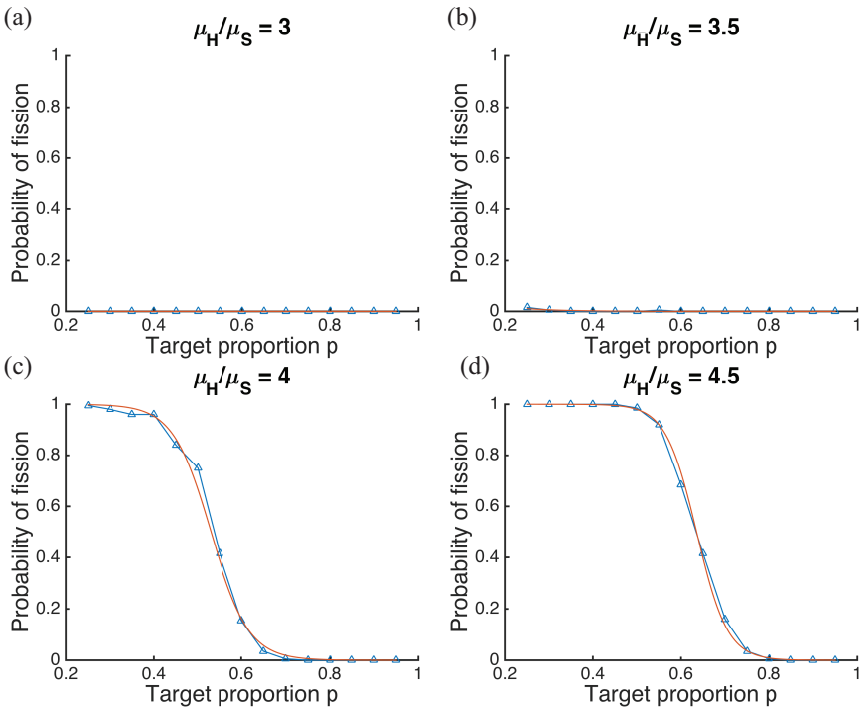

Fig. 8 The relationship between the probability of fission and target proportion. Simulation data (blue triangles) and the modelled logistic functions (red lines) for stiffness ratio values μ_H/μ_S of (a) $\mu_H/\mu_S = 3$, (b) $\mu_H/\mu_S = 3.5$, (c) $\mu_H/\mu_S = 4$ and (d) $\mu_H/\mu_S = 4.5$. The sigmoidal function appears to travel along the $p-$axis as μ_H/μ_S is increased.

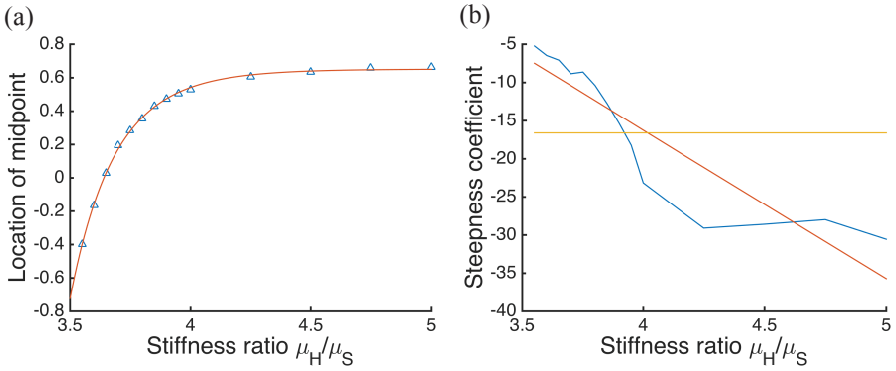

Fig. 9 Modelling the probability of fission. (a) The points of inflection of the fitted logistic functions (blue triangles) can be modelled as a function of the stiffness ratio μ_H/μ_S. A power series model (red) was fitted to the set of points. (b) The steepness coefficients (blue) were modelled by taking the average value (yellow). The linear regression fit (red) has also been displayed.

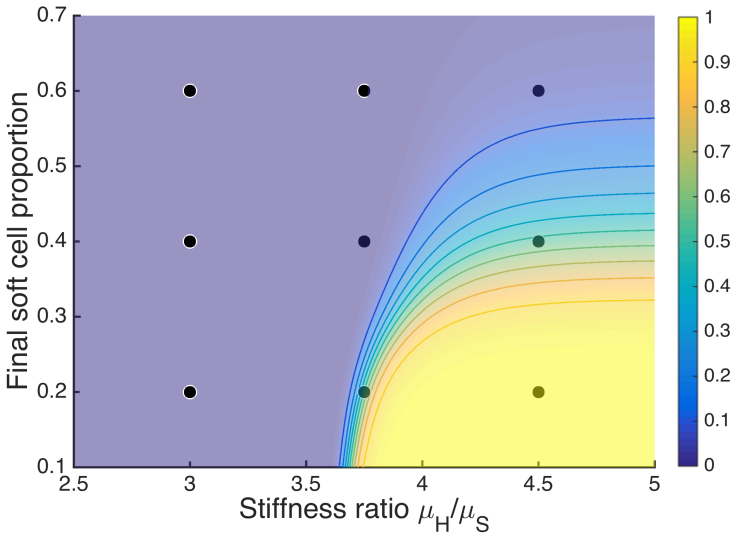

Fig. 10 The full interpolated contour of fission probabilities. Regions of probabilities are coloured in the same manner as Figure 7. The shape of the epithelial layer was analysed for all combinations of $\mu_H/\mu_S = 3,\ 3.75$ and 4.5 and steady state soft cell proportions of 0.2, 0.4 and 0.6. These points have been marked with a black circle on the contour and were chosen in order to investigate all possible significant behaviour of the epithelial layer.

3.2 Fission is due to increases in the stiffness or number of hard cells

The contour of fission probabilities displayed in Figure 10 reveals a phase space comprising regions of crypt homeostasis and crypt buckling. The diagram further suggests that different combinations of soft cell proportion and hard cell stiffness can lead to the same mechanical outcome. However, the phase space does not provide any information about the nature of fission in the model. In particular, the contour does not tell us whether different regions of non-zero fission probability correspond to different types of deformation in the epithelial layer.

Additional simulations were run on a subset of parameter values in order to investigate the nature of deformation in the epithelial layer. This subset of values is shown in Figure 10 and was chosen to capture all significant types of deformation in the layer. For example, for $\mu_H/\mu_S = 4.5$, the epithelial tissue will always undergo fission for low soft cell proportions, but as the proportion of softer cells increases, the frequency of fission is reduced until the layer is always stable. The distribution of circularity values was analysed for these points. For each point, histograms with ten evenly spaced bins from zero to one were produced from 100 independent simulations. These histograms are displayed in Figure 11 at the corresponding location of each steady state proportion and stiffness ratio. In regions where fission is non-existent, corresponding to

epithelial layers with low stiffness ratio values or high soft cell proportions, the circularity distributions are centred close to one. For a given soft cell proportion, as the stiffness ratio μ_H/μ_S increases, the mass of the circularity distribution becomes skewed towards zero. Similar behaviour is witnessed for higher values of μ_H/μ_S as proportion of soft cells decreases. This results in an increase in fission incidence.

To gain insight into the shape of the epithelial layer, for each histogram five of the cross sections were drawn randomly from the bin with the most frequent count and overlaid on top of each other. These representative spatial portraits are also shown in Figure 11 and are plotted on axes of the same size to represent the physical differences between different parameter combinations. Distributions centred closer to unity reflect a stable circular shape, indicating homeostasis, while distributions biased towards zero indicate the layer has buckled and crypt buds have formed. Furthermore, although different parameter value combinations can lead to the same probability of fission and a similar circularity distribution, the corresponding layers may differ. For example, the distribution of circularities for $\mu_H/\mu_S = 3.75$ and a soft cell proportion of 0.2 is similar to the distribution for $\mu_H/\mu_S = 4.5$ and a proportion of 0.4, but the epithelial layers for $\mu_H/\mu_S = 3.75$ are larger in circumference. This is because there is a greater number of stiffer hard cells in these layers, resulting in an increase of the net force exerted on the surrounding non-epithelial cells by the epithelium.

Figure 11 shows that the probability of crypt fission is directly linked to the type of deformation in the layer. For example, in regions where hard cells are 4.5 times stiffer than soft cells and constitute the majority of the cell population, the layer exhibits behaviour similar to crypt fission and budding. However, when the proportion of soft cells is greater and the probability of fission is smaller, the layer exhibits deformation more akin to buckling. This new spatial insight gleaned from the histograms and organoid portraits presents an interesting biological interpretation. For an epithelial layer in homeostasis to undergo crypt fission, there are two possibilities. One is for the number of much stiffer hard cells to increase, which decreases the overall proportion of soft cells in the layer. Alternatively, fission can also occur when there is already a high proportion of stiffer cells and the stiffness of these cells increases further while their number remains approximately constant.

3.3 Cell patterning correlates with the occurrence of fission

Having explored the spatial consequences of cells with different mechanical properties in the epithelial layer, we examine the effect of fission on the distribution of cells in the ring. For the same subset of parameters marked in Figure 10, we consider each epithelial layer as an unfolded one-dimensional chain with periodic boundaries. For a pair of soft cell proportion and stiffness ratio values, for each cell in the ring the cell types of the five right neighbours are recorded.This allows the calculation of the probability that the right neigh-

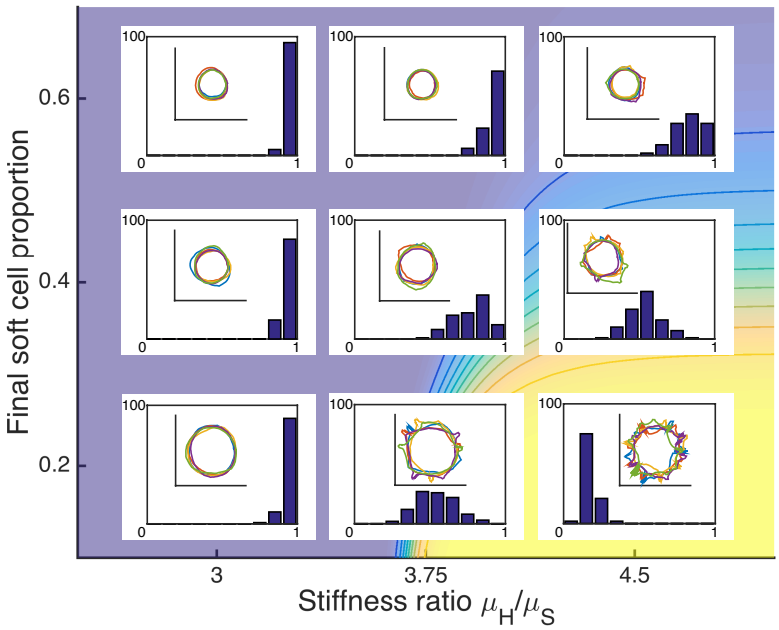

Fig. 11 The nature of deformation in the epithelial layer. Histograms of the circularity values have been displayed for the parameter value combinations indicated in Figure 10. Each histogram contains ten bins, evenly spaced from zero to one. Furthermore, for the circularity bin with the highest count, five of the epithelial layers with such circularities have been overlaid to give an indication of shape. The right column uses the same data as Langlands et al. (2016) (reproduced with permission).

bours of a soft cell will also be soft cells (or similarly for hard cells). In effect, we are testing the model for complete spatial randomness: if mechanical heterogeneity has no effect on the distribution of cell types, then we expect the probability of cell type occupancy for a cell site to be independent of the other cell sites. Thus, if the model exhibited complete spatial randomness, the probabilities of site occupancy would be constant and equal to the final soft (hard) cell proportion.

The resultant neighbourhood correlation functions are shown in Figure 12. For all parameter combinations, the most apparent effect of mechanical heterogeneity is on the adjacent right neighbour of soft cells. For all stiffness ratio values μ_H/μ_S, we see that when there are more hard cells than soft cells in the layer, the probability that a soft cell is adjacent to another soft cell is much lower than expected. Although this probability increases as the proportion of soft cells in the layer increases, the probability of the adjacent neighbour of a soft cell also being a soft cell is consistently lower than the probabilities for the other four neighbouring sites. The reason for this low nearest-neighbour probability is that when a soft cell divides symmetrically, one of the daughter cells

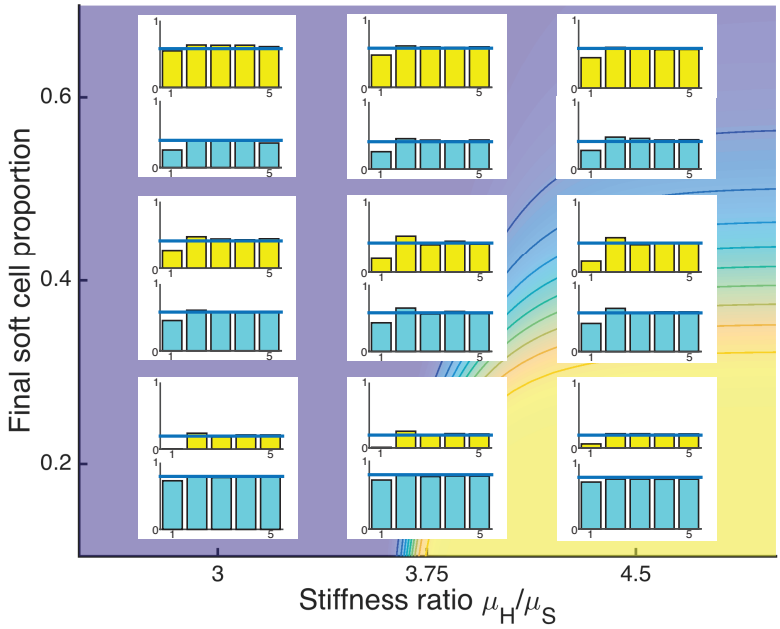

Fig. 12 The effect of crypt fission on cell patterning. Distributions of the average neighbouring site occupancies for soft and hard cells have been plotted. For each data point, the upper (yellow) histograms correspond to the average soft cell occupancies for the five neighbouring sites to the right of a soft cell, while the lower (blue) histograms correspond to the average hard cell occupancies for a hard cell's five right neighbours. The dark blue lines mark the steady state soft and hard cell proportions on he upper and lower histograms respectively. The bottom row uses the same data as Langlands et al. (2016) (reproduced with permission).

will likely be pushed out due to the resulting force exerted by a neighbouring hard cell. This is consistent with the observation that the nearest-neighbour probability also decreases as the stiffness ratio increases; that is, when the hard cells are much stiffer than the stem cells. Contrastingly, when the soft cell proportion is 0.2, we see an increase in the adjacent site probability for $\mu_H/\mu_S = 4.5$, when crypt fission occurs. The increase is caused by how buds develop during crypt fission: in our model, cells in a bud cannot be pushed out into the lumen and experience anoikis. Soft cells created through symmetric division will hence be less likely to be ejected immediately.

For hard cells, we see a similar phenomenon when the proportion of hard cells in the layer is low. Again, the probability that the adjacent right cell is also a hard cell is consistently lower than the other neighbouring site occupancies and the expected hard cell proportion in the layer. This suggests that in the steady state regime, a soft cell is most likely to be located next to a hard cell. Although the adjacent site occupancy is consistently lower than the other neighbour occupancies, as it is for soft cells, it is not nearly as low as the

adjacent site probability for soft cells. This discrepancy arises from the higher stiffness of hard cells, as they are less likely to be pushed out of the chain. This alternating pattern of hard and soft cells is witnessed in the small intestinal crypt base (Langlands et al., 2016), but it is difficult to make any definitive conclusions from our results, as our model assumes a two-dimensional cross-sectional geometry, where cells cannot move past each other.

The results displayed in Figure 12 demonstrate that the mechanical differences between soft and hard cells have a clear effect on the distributions of cells in the epithelial layer. We are more likely to see long bands of hard cells than long bands of soft cells in the model. Moreover, a soft cell is far more likely to be adjacent to a hard cell than another soft cell. Note that if soft and hard cells were identical, that is, if the stiffness ratio $\mu_H/\mu_S = 1$, we do not see this behaviour and the distribution is instead completely random.

3.4 Heterogeneity in cell size correlates with layer shape

Even though different cell types in tissue have different sizes, here we have modelled all cells to be the same size. For example, in the crypt, differentiated cells are larger than undifferentiated stem cells; indeed, the cross-sectional area of Paneth cells in the small intestinal crypt base is at least twice that of stem cells (Langlands et al., 2016). However, in the model, there is no one parameter for cell size; instead, cell size is the result of mechanical cell interactions. We analysed the average cell size of soft and hard cells on the same parameter values analysed previously to determine which model parameters affected size the most. The size of a cell was measured by the area of its Voronoï region in the model.

We found that across the parameter space, the average size of hard cells was consistently greater than that of soft cells, on average 1.2 times as large as soft cells, showing that a difference in cell size emerged in our model, due to the variable cell stiffness. The lowest difference between hard and soft cells size occurred when the soft cell proportion was 0.2, with a stiffness ratio of $\mu_H/\mu_S = 3$,, corresponding to an average cell area ratio of 1.08. Contrastingly, the highest average cell area ratio, 1.4, when the soft cell proportion was 0.6, with $\mu_H/\mu_S = 4.5$. For the former scenario, the epithelial layer is a large circle, while for the latter, the layer is a small circle (see insets in Figure 11). When the layer is a tightly-packed circle, the repulsion forces exerted by hard cells on neighbouring cells is enhanced due to spatial constraints. Decreasing the stiffness ratio decreases the repulsion forces, but increasing the proportion of hard cells increases the net force exerted by the layer on the surrounding non-epithelial cells, resulting in an increased layer circumference. This reduces the influence of hard cells on neighbouring soft cells, allowing them to relax to a larger equilibrium area, reducing the area ratio.

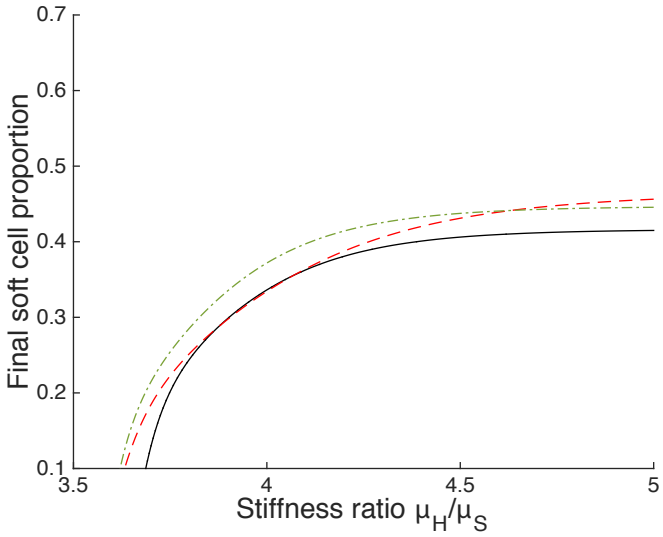

Fig. 13 The effect of increasing the adhesion of hard cells on the likelihood of fission. The contour corresponding to a fission probability of 0.5 has been plotted for the $\eta_H = 1$ (black, solid), $\eta_H = 1.3$ (red, dashed) and $\eta_H = 2$ (orange, dot-dashed) cases. Increasing η_H widens the region of fission occurrence.

3.5 Increasing the biomechanical differences between cells increases the probability of fission

We primarily focused on the effect of cell stiffness on epithelial layer stability. An important biomechanical factor we have yet to consider but is often considered in the literature is the variable adhesion of cells (Osborne et al., 2010; Mirams et al., 2012). In the crypt, it has been shown that differentiated cells exhibit higher cell-substrate adhesion than undifferentiated cells in homeostasis (Beaulieu, 1992). It has also been shown that cell-cell adhesion is lower in cancerous cells than in non-cancerous stem cells (Frixen et al., 1991). In the small intestinal crypt base, Langlands et al. (2016) found that Paneth cells contain about 1.3 times more $\beta 4$ integrin (adhesion molecules) on their basal surfaces than stem cells, suggesting that Paneth cells are 1.3 more adhesive than stem cells. In our model, for a given cell i, the drag coefficient η_i (Equation (1)) incorporates aspects of the drag and adhesion experienced by the cell, including cell-cell and basal adhesion. If we were to treat hard cells as Paneth cells, this would suggest that $\eta_H = 1.3\eta_S = 1.3$. This led us to run further *in silico* experiments with this altered hard cell drag coefficient. Our aim was to observe the change to the contour of fission probabilities produced in Figure 10. We thus performed the same analysis outlined in Sections 2.8–3.1 for this altered drag coefficient. We note that all other aspects of the model were unchanged. We also analysed the model for $\eta_H = 2$ to observe the effect of altering cell adhesion more significantly.

Figure 13 demonstrates the effect of increasing the adhesiveness of hard cells on the shape of the fission probability contours. The 0.5 probability contour has been plotted for each η_H case, with the black line taken from Figure 10. From this, we observe that increasing η_H increases the region where fission occurs. However, the different behaviours of the fission region borders indicates that there is no clearly-defined relationship between cell adhesion and the probability of crypt fission. Furthermore, the behaviour of the epithelial layer did not appear to change significantly in regions of fission for the different drag coefficients (results not shown). Ultimately, these results suggest that while increasing adhesion does increase the levels of fission slightly, changing the adhesion of hard cells does not affect the behaviour of the epithelial layer significantly.

4 Discussion

The aim of this paper was to adapt a multicellular model of a deformable crypt to an abstracted study of crypt fission, focusing on the mechanical factors leading to its onset. Building on the work of Dunn et al. (2012a,b), we presented a computational model of a connected epithelial layer that could be interpreted as the cross section of either a three-dimensional organoid or two conjoined crypt bases. Observing the co-existence of biomechanically distinct stem and differentiated cells in crypt bases (Paneth cells in the small intestine, cKit$^+$ cells in the colon; see Rothenberg et al. (2012)) and fissioned organoid buds, we introduced two interacting cell subpopulations with different mechanical properties into the epithelial layer, focusing primarily on cell stiffness with a brief exploration of cell adhesion and size. Varying the relative stiffness of cells was sufficient to initiate budding akin to crypt fission in the epithelial layer.

Both the proportions and relative stiffness of cell types affected the likelihood of crypt fission occurring in the layer. Using interpolation, we could model the probability of crypt fission as a smoothly varying function of the steady state soft cell proportions and stiffness ratios, demonstrating that crypt buckling could be initiated in a number of ways. Spatial analysis of the model revealed that the nature of deformation in the model varied across the parameter space. These deformations affected both the distribution of cells and cell size heterogeneity in the epithelial layer. We found that increasing the adhesiveness of hard cells increased the chance of fission, but did not have a significant effect on the type of deformations witnessed.

The results suggest two primary scenarios that can cause a crypt to undergo fission. In the first scenario, stiffer cells dominating the crypt population increase further in stiffness while remaining relatively fixed in proportion. In the second, the number of stiffer cells in the crypt base increases over time. This scenario is perhaps more biologically realistic and, in the context of stem and Paneth cells in the small intestine, has indeed been verified in recent experimental work (Langlands et al., 2016).

Analysing the epithelial layer during fission showed that different proportions of stiffer cells correlated with different types of crypt fission. Epithelial layers with high proportions of stiffer cells exhibited budding, found mainly in healthy crypts, while layers with lower proportions of stiffer cells exhibited buckling, which is more reminiscent of cancerous crypts. This suggests that cell stiffness also plays a role in adenoma formation. While the stiffness of cancerous cells in the crypt has not been considered, the ability of cancer cells to alter the stiffness of the surrounding extracellular to facilitate metastasis is well established (Denys et al., 2008; Baker et al., 2013).

The general nature of our modelling framework allows us to interpret the epithelial layer in a number of ways. For discussing biological implications, we have primarily interpreted the two cell subpopulations as stem and Paneth or cKit$^+$ cells in the crypt base. However, we could also interpret the model as describing healthy and cancerous cells or more general differentiated and undifferentiated cells. To consider specific cell types, more model parameters need to be added. For example, if we were to focus on modelling cancerous stem cells in the epithelial layer, we would have to consider changing a number of parameters. While it is known that cancerous cells are less adhesive to other cells than healthy stem cells in the crypt (Frixen et al., 1991), the changes in cell stiffness during colorectal cancer development are not known. In addition, as cancer cells can remodel the surrounding extracellular matrix (Denys et al., 2008; Baker et al., 2013) during invasion, it could be of value to model changes in stiffness using the basement membrane stiffness parameter β.

We modelled the proliferation and differentiation of each cell using a stochastic based cell cycle model that is independent of spatial, cell type, or cell signalling. However, Wnt and Notch signalling pathways are important in determining cell fate (Sato et al., 2011) and increased Wnt signalling is linked to colorectal cancer (Reya and Clevers, 2005). It will therefore be important to explore the effect of more sophisticated sub-cellular mechanisms on deformation in the epithelial layer in future work.

In this study we have focused on the mechanical basis of crypt fission. It has been proposed that the process of fission is initiated by cell patterning in the base of the crypt (Langlands et al., 2016) and as discussed earlier one cannot represent cell sorting in the current model (as it is representing the epithelial layer in one dimension only). In order to investigate this phase of fission we could extend the existing deformable model to a two-dimensional epithelial layer (i.e. a three-dimensional simulation) where such cell sorting could be included as an initiating phase of the deformation.

We have presented a multiscale model of an epithelial layer that can be used to study crypt fission in a robust manner. We have shown that crypt fission can be initiated through model parameter changes that quantify the relative stiffness of epithelial cells and the proportions of different cell subpopulations in the layer. Furthermore, the mechanism underlying fission and results are consistent with recent experimental findings. Importantly, the model retains a sufficient level of abstraction to allow us to interpret our findings in a variety of biological contexts. Conclusions can be inferred for both *in vivo* crypts and

in vitro organoids, and for both crypt homeostasis and colorectal cancer. As we have not had to resort to any excessively complex modelling approaches, our model can be extended straightforwardly in a number of ways for further exploration of crypt buckling and fission.

Acknowledgements

A.A.A, B.D.H and K.A.L were supported by the Australian Research Council (DP110100795). A.A.A and J.M.O were funded by a University of Melbourne ECR Grant.

References

Alberts B, Johnson A, Lewis J, Raff M, Roberts K, Walter P (2002) Molecular Biology of the Cell. Garland Science, New York

Aurenhammer F, Klein R, Lee DT, Klein R (2013) Voronoi diagrams and Delaunay triangulations, vol 8. World Scientific

Baker A, Bird D, Lang G, Cox TR, Erler J (2013) Lysyl oxidase enzymatic function increases stiffness to drive colorectal cancer progression through FAK. Oncogene 32(14):1863–1868

Barker N, van Es JH, Kuipers J, Kujala P, van den Born M, Cozijnsen M, Haegebarth A, Korving J, Begthel H, Peters PJ, et al. (2007) Identification of stem cells in small intestine and colon by marker gene Lgr5. Nature 449(7165):1003–1007

Beaulieu JF (1992) Differential expression of the VLA family of integrins along the crypt-villus axis in the human small intestine. Journal of Cell Science 102(3):427–436

Björck A (1996) Numerical Methods For Least Squares Problems. SIAM

Buske P, Galle J, Barker N, Aust G, Clevers H, Loeffler M (2011) A comprehensive model of the spatio-temporal stem cell and tissue organisation in the intestinal crypt. PLoS Computational Biology 7(1):e1001,045

Buske P, Przybilla J, Loeffler M, Sachs N, Sato T, Clevers H, Galle J (2012) On the biomechanics of stem cell niche formation in the gut–modelling growing organoids. FEBS Journal 279(18):3475–3487

Cairnie AB, Millen BH (1975) Fission of crypts in the small intestine of the irradiated mouse. Cell Proliferation 8(2):189–196

Cheng H, Bjerknes M (1985) Whole population cell kinetics and postnatal development of the mouse intestinal epithelium. The Anatomical Record 211(4):420–426

Dallon JC, Othmer HG (2004) How cellular movement determines the collective force generated by the Dictyostelium discoideum slug. Journal of Theoretical Biology 231(2):203–222

Denys H, Derycke L, Hendrix A, Westbroek W, Gheldof A, Narine K, Pauwels P, Gespach C, Bracke M, De Wever O (2008) Differential impact of TGF-β

and EGF on fibroblast differentiation and invasion reciprocally promotes colon cancer cell invasion. Cancer Letters 266(2):263–274

Drasdo D, Loeffler M (2001) Individual-based models to growth and folding in one-layered tissues: intestinal crypts and early development. Nonlinear Analysis: Theory, Methods & Applications 47(1):245–256

Dunn SJN, Appleton PL, Nelson SA, Näthke IS, Gavaghan DJ, Osborne JM (2012a) A two-dimensional model of the colonic crypt accounting for the role of the basement membrane and pericryptal fibroblast sheath. PLoS Computational Biology 8(5):e1002,515, DOI 10.1371/journal.pcbi.1002515

Dunn SJN, Fletcher AG, Chapman SJ, Gavaghan DJ, Osborne JM (2012b) Modelling the role of the basement membrane beneath a growing epithelial monolayer. Journal of Theoretical Biology 298:82–91

Dunn SJN, Näthke IS, Osborne JM (2013) Computational models reveal a passive mechanism for cell migration in the crypt. PloS One 8(11):e80,516

Edwards CM, Chapman SJ (2007) Biomechanical modelling of colorectal crypt budding and fission. Bulletin of Mathematical Biology 69(6):1927–1942

Frixen UH, Behrens J, Sachs M, Eberle G, Voss B, Warda A, Löchner D, Birchmeier W (1991) E-cadherin-mediated cell-cell adhesion prevents invasiveness of human carcinoma cells. The Journal of cell biology 113(1):173–185

Galle J, Loeffler M, Drasdo D (2005) Modeling the effect of deregulated proliferation and apoptosis on the growth dynamics of epithelial cell populations in vitro. Biophysical Journal 88(1):62–75

Greaves LC, Preston SL, Tadrous PJ, Taylor RW, Barron MJ, Oukrif D, Leedham SJ, Deheragoda M, Sasieni P, Novelli MR, et al. (2006) Mitochondrial DNA mutations are established in human colonic stem cells, and mutated clones expand by crypt fission. Proceedings of the National Academy of Sciences 103(3):714–719

Hannezo E, Prost J, Joanny JF (2011) Instabilities of monolayered epithelia: shape and structure of villi and crypts. Physical Review Letters 107(7):078,104

Hosmer Jr DW, Lemeshow S (2004) Applied Logistic Regression. John Wiley & Sons

Langlands AJ, Almet AA, Appleton PL, Newton IP, Osborne JM, Näthke IS (2016) Paneth cell-rich regions separated by a cluster of Lgr5+ cells initiate crypt fission in the intestinal stem cell niche. PLoS Biology 14(6):e1002,491, DOI 10.1371/journal.pbio.1002491

Meineke FA, Potten CS, Loeffler M (2001) Cell migration and organization in the intestinal crypt using a lattice-free model. Cell Proliferation 34(4):253–266

Mirams GR, Fletcher AG, Maini PK, Byrne HM (2012) A theoretical investigation of the effect of proliferation and adhesion on monoclonal conversion in the colonic crypt. Journal of Theoretical Biology 312:143–156

Mirams GR, Arthurs CJ, Bernabeu MO, Bordas R, Cooper J, Corrias A, Davit Y, Dunn SJN, Fletcher AG, Harvey DG, et al. (2013) Chaste: an open source C++ library for computational physiology and biology. PLoS Computational Biology 9(3):e1002,970

Nelson M, Howard D, Jensen O, King J, Rose F, Waters S (2011) Growth-induced buckling of an epithelial layer. Biomechanics and Modeling in Mechanobiology 10(6):883–900

Osborne JM, Walter A, Kershaw SK, Mirams GR, Fletcher AG, Pathmanathan P, Gavaghan DJ, Jensen OE, Maini PK, Byrne HM (2010) A hybrid approach to multi-scale modelling of cancer. Philosophical Transactions of the Royal Society A: Mathematical, Physical and Engineering Sciences 368(1930):5013–5028

Park HS, Goodlad RA, Wright NA (1995) Crypt fission in the small intestine and colon. a mechanism for the emergence of G6PD locus-mutated crypts after treatment with mutagens. American Journal of Pathology 147(5):1416

Pin C, Watson AJ, Carding SR (2012) Modelling the spatio-temporal cell dynamics reveals novel insights on cell differentiation and proliferation in the small intestinal crypt. PLoS One 7(5):e37,115

Pin C, Parker A, Gunning AP, Ohta Y, Johnson IT, Carding SR, Sato T (2015) An individual based computational model of intestinal crypt fission and its application to predicting unrestrictive growth of the intestinal epithelium. Integrative Biology 7(2):213–228

Pitt-Francis J, Pathmanathan P, Bernabeu MO, Bordas R, Cooper J, Fletcher AG, Mirams GR, Murray PJ, Osborne JM, Walter A, et al. (2009) Chaste: a test-driven approach to software development for biological modelling. Computer Physics Communications 180(12):2452–2471

Preston SL, Wong WM, Chan AOO, Poulsom R, Jeffery R, Goodlad RA, Mandir N, Elia G, Novelli M, Bodmer WF, et al. (2003) Bottom-up histogenesis of colorectal adenomas origin in the monocryptal adenoma and initial expansion by crypt fission. Cancer Research 63(13):3819–3825

Reya T, Clevers H (2005) Wnt signalling in stem cells and cancer. Nature 434(7035):843–850

Rothenberg ME, Nusse Y, Kalisky T, Lee JJ, Dalerba P, Scheeren F, Lobo N, Kulkarni S, Sim S, Qian D, et al. (2012) Identification of a cKit+ colonic crypt base secretory cell that supports Lgr5+ stem cells in mice. Gastroenterology 142(5):1195–1205

Sato T, Vries RG, Snippert HJ, van de Wetering M, Barker N, Stange DE, van Es JH, Abo A, Kujala P, Peters PJ, et al. (2009) Single Lgr5 stem cells build crypt villus structures in vitro without a mesenchymal niche. Nature 459(7244):262–265

Sato T, van Es JH, Snippert HJ, Stange DE, Vries RG, van den Born M, Barker N, Shroyer NF, van de Wetering M, Clevers H (2011) Paneth cells constitute the niche for Lgr5 stem cells in intestinal crypts. Nature 469(7330):415–418

Snippert HJ, Schepers AG, van Es JH, Simons BD, Clevers H (2013) Biased competition between Lgr5 intestinal stem cells driven by oncogenic mutation induces clonal expansion. EMBO reports p e201337799

Süli E, Mayers DF (2003) An Introduction to Numerical Analysis. Cambridge University Press

Trier JS, Allan CH, Abrahamson DR, Hagen SJ (1990) Epithelial basement membrane of mouse jejunum. Evidence for laminin turnover along the entire

crypt-villus axis. Journal of Clinical Investigation 86(1):87

Van Leeuwen IMM, Mirams GR, Walter A, Fletcher AG, Murray PJ, Osborne JM, Varma S, Young SJ, Cooper J, Doyle B, et al. (2009) An integrative computational model for intestinal tissue renewal. Cell Proliferation 42(5):617–636

Wright NA, Alison M (1984) The Biology of Epithelial Cell Populations, vol 1–2. Oxford University Press, USA

Zaman MH, Trapani LM, Sieminski AL, MacKellar D, Gong H, Kamm RD, Wells A, Lauffenburger DA, Matsudaira P (2006) Migration of tumor cells in 3D matrices is governed by matrix stiffness along with cell-matrix adhesion and proteolysis. Proceedings of the National Academy of Sciences 103(29):10,889–10,894

Žunić J, Hirota K (2008) Measuring shape circularity. Progress in Pattern Recognition, Image Analysis and Applications pp 94–101